



ORIGINAL ARTICLE

High sensitive assay of formaldehyde using resonance light scattering technique based on carbon dots aggregation



Shuai Zhang^a, Xiaoyu Fan^a, Shuhan Jiang^a, Dou Yang^a, Min Wang^a, Tao Liu^a, Xiaodong Shao^b, Shuhao Wang^a, Guangzhi Hu^{c,*}, Qiaoli Yue^{a,*}

^a School of Chemistry and Chemical Engineering, Shandong Provincial Key Laboratory of Chemical Energy Storage and Novel Cell Technology, Liaocheng University, Liaocheng 252059, China

^b State Key Laboratory for Performance and Structure Safety of Petroleum Tubular Goods and Equipment Materials, Tubular Goods Research Institute, Xian 710077, China

^c Department of Physics, Umeå University, S-901 87 Umeå, Sweden

Received 13 January 2023; accepted 1 March 2023

Available online 8 March 2023

KEYWORDS

Formaldehyde detection;
Carbon dots;
Schiff-base reaction;
Resonance light scattering;
Food samples

Abstract Formaldehyde (FA) is widely used in industry and also common in daily life. Finding an efficient method to determine FA is quite an industrial challenge. Herein, a novel method based on a resonance light scattering (RLS) technique was developed for the detection of FA with high sensitivity. Carbon dots (CDs) were used as RLS probes. CDs were obtained via one-pot solvothermal treatment from *o*-phenylenediamine. CDs showed yellow fluorescence with a quantum yield of 0.41. Due to the multiple amino groups on the surface of CDs, FA can be captured easily by formation of a covalent C = N bond based on the Schiff-base reaction. Owing to the covalent crosslinking, CD nanoparticles aggregated, and even formed precipitate. The aggregation of CDs induced RLS enhancement, where the RLS increment was linearly related to the concentration of FA ranging from 4 nM to 1.6 mM, with a limit of detection (LOD) of 1.6 nM. In comparison with many previous reports, the present RLS method showed a wider linear range and lower LOD. Furthermore, the RLS system was successfully used to detect FA in real food samples. The proposed system has prospective applicability in the detection of FA in food fields.

© 2023 The Authors. Published by Elsevier B.V. on behalf of King Saud University. This is an open access article under the CC BY-NC-ND license (<http://creativecommons.org/licenses/by-nc-nd/4.0/>).

1. Introduction

Formaldehyde (FA) is a colorless, flammable gas at room temperature and has a strong odor. FA is widely used in the

manufacture of composite wood products, building materials, household products, medicines, cosmetics and pesticides. Exposure to FA may cause adverse health effects such as irritation of the skin, eyes, nose and throat. It is reported that

* Corresponding authors.

E-mail addresses: guangzhi.hu@umu.se (G. Hu), yueqiaoli@lcu.edu.cn (Q. Yue).

the inhalation of air containing FA can lead to severe diseases, even at the ppm level (Luo et al., 2018; Park et al., 2012). There are also some serious health issues for human when they consume food contaminated by FA such as vomiting, pain or coma (Nordin et al., 2011). According to the report of European Union, the minimum daily exposure to FA is 100 mg kg^{-1} from animal and plant origin food (Zhang et al., 2022a, 2020b), and it is strictly forbidden to use formalin adulteration in China (Aquilina et al., 2014). Therefore, developing a sensitive, selective, and convenient method of detecting FA is urgent.

Various methods of determining FA in gas samples have been reported, including spectrophotometry (Gorrotxategi-Carbajo et al., 2013), electrochemistry (Zhang et al., 2020a, 2020b), chemiluminescence (Song et al., 2009), fluorescence (Liu et al., 2019; Wang et al., 2021), and imaging (Liu et al., 2019) techniques. Various materials have been employed for FA detection, such as ZIF-90-LW (Wen et al., 2020), naphthalimide (Bi et al., 2018), CuO/Cu/TiO₂ nanotubes (Zhang et al., 2020a, 2020b), egg white/ZnO (Padmalaya et al., 2022), carbon dots (CDs) (Qu et al., 2020; Lin et al., 2022; Kim et al., 2021; Liu et al., 2021; Li et al., 2023; Zhao et al., 2022; Hu and Gao, 2020), SnSO₄/ZnO (Chang et al., 2018), C₆₀-encapsulated TiO₂ (Gakhar and Hazra, 2021), ZnSnO₃ porous nanostructures (Du et al., 2021), and RGO/HA-HCl (Zhou et al., 2020). However, there are still some limits for these methods such as high cost, high toxic reagent use, as well as the only use in aqueous media or vapor. Therefore, how to achieve high sensitivity to determine FA both in liquids and gases is still challenging.

Schiff-base reactions have played a major role, and still have a significant function in the development of inorganic chemistry (Zaltariov and Cazacu, 2020). The ligands that are most commonly used for Schiff-base reactions are aldehydes or ketones and primary amines, Schiff-base reactions are widely used to form complexes with different architectures, and it has an extensive application (Visuvamithiran et al., 2013). There are a few reports in which Schiff-base reactions are exploited for sensing analytes, such as Schiff-base reaction induced detection of dopamine based on the Pt₄₁Rh₅₉ alloy/ZIF-90 nanocomposite and the FA based on the CD-ND (Chen et al., 2019a, 2019b).

A novel resonance light scattering (RLS) method based on CDs is constructed for the sensitive detection of FA. Due to its high sensitivity, rapidity, and convenience, the RLS technique has attracted much interest in analytical and environmental chemistry (Chen et al., 2017, 2018; Liu et al., 2018; Lu et al.,

2006; Luo et al., 2019, 2020, Wang et al., 2017, 2019b; Yang et al., 2017). RLS can be carried out on a common fluorescence spectrometer with inexpensive and safe materials and reagents (Hou et al., 2017; Yang et al., 2017). RLS spectra can be easily obtained by synchronous scanning with the same excitation and emission wavelength. The RLS signal can be enhanced by enlargement of the molecule or particle via assembly of small molecules or particles. Various RLS approaches were constructed for analytes based on increase or decrease of RLS signal.

CDs were obtained by a simple hydrothermal method using 1,2-diaminobenzene (*o*-phenylenediamine, OPD) as precursor material. CDs can be freely dispersed in aqueous medium without aggregation. Due to abundant amino groups on the surface of CDs, FA can be easily captured by CDs owing to the covalent crosslink via Schiff-base reaction. The covalent crosslink among nanoparticles led to the aggregation of CDs and even precipitate immediately. The aggregation of CDs induced the RLS enhancement. The RLS increase was linearly responsive to the concentration of FA, enabling the sensitive and selective sensing of FA (Scheme 1).

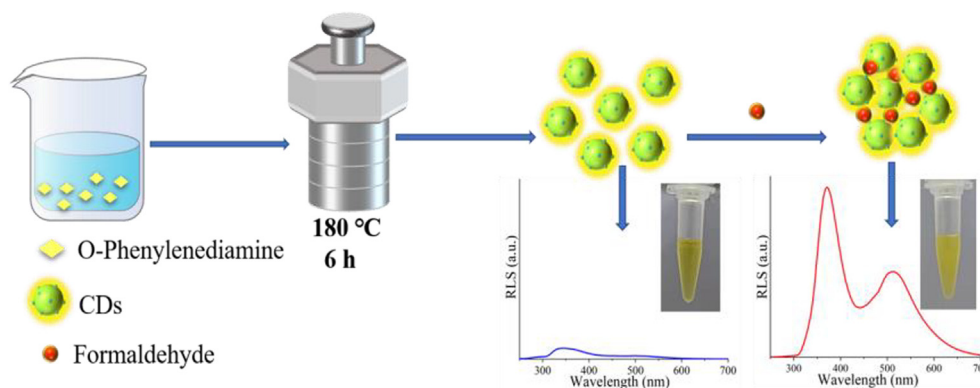
2. Materials and methods

2.1. Chemicals and materials

Glyoxal solution (GA) (40 wt% in H₂O and H₂O₂ (HP) ($\geq 30\%$)) was ordered from Shanghai Perfemiker Material Technology Co., Ltd. FA (36%-38%), ethanol (EtOH) ($\geq 99.8\%$), methanol (MeOH) ($\geq 99.5\%$) and acetone (Ace) ($\geq 99.5\%$) were purchased from Yantai Far Eastern Fine Chemical Co., Ltd. OPD ($\geq 99.5\%$). Acetaldehyde (AA) ($\geq 40\%$) was obtained from Tianjin Kermel Reagent Co., Ltd (Tianjin, China). Propionaldehyde (PA) ($\geq 99\%$) and butyraldehyde (BA) ($\geq 97\%$) were ordered from Shanghai Macklin Biochemical Co., Ltd. The small shrimps were bought from a supermarket on campus. All chemicals were used without further purification. Deionized (DI) water was used throughout the experiments from Milli-Q water purified system.

2.2. Synthesis of CDs

The yellow-emitting CDs were obtained via a simple hydrothermal treatment and the experimental conditions



Scheme 1 Synthesis of CDs and detection of FA.

including mass of precursors, hydrothermal reaction time and temperature were investigated by reference to literatures (Zhao et al., 2019; Vedernikova et al., 2022; Papaioannou et al., 2019, Gao et al., 2021). The reaction time affects the morphology of CDs, no nanometer-sized particles were observed under the reaction time of 6 h. So the reaction time for the synthesis of CDs was 6 h (Papaioannou et al., 2019). Briefly, 0.036 g OPD was introduced into 10 mL deionized water, and then heated in a Teflon-sealed autoclave reactor at 180 °C for 6 h. And then the product solution was filtered with a 0.22 μm filter membrane and dialyzed with dialysis bag (molecular weight cutoff ≈ 500 Da, for 12 h). CDs solution was heated in a vacuum drying oven at 60 °C for 24 h to obtain solid product. Finally, the CDs was stored in a refrigerator at 4 °C for subsequent use.

2.3. Characterization of CDs

The transmission electron microscope (TEM) images were recorded on a JEM 2100 electron microscope. TEM worked with an acceleration voltage of 200 kV, and a copper grid was used for CDs suspension. (JEOL Ltd, Japan). Dynamic light scattering (DLS) data for CDs were acquired using a Zetasizer Nana-ZS System (MPI Ltd, UK). Fourier-transform infrared (FT-IR) spectra were acquired using pressed KBr pellets on a Nicolet 6700 spectrometer (Thermo Scientific Ltd,

USA). The powder X-ray diffraction (XRD) measurement was performed on a D/Max-2500 Diffractometer with Cu K α radiation ($\lambda = 0.15406$ nm) at 2θ ranging between 5° and 80°. X-ray photoelectron spectroscopy (XPS) measurements were performed with a K-Alpha spectrometer (Thermo Scientific Ltd, USA).

2.4. Detection of FA in aqueous media

CDs (250 μL, 1 mg mL⁻¹) and FA solutions (1 μL) with different concentrations were placed in 1.5 mL centrifuge tubes and allowed to react at room temperature for 18 min. Subsequently, the RLS spectra of the mixture, as well as that of the blank were recorded. To investigate the specificity of the CDs for FA detection, a series of materials with similar structure as FA (AA, PA, BA, GA, HP, MeOH, EtOH, Ace, and Glu) were added to CDs solution and RLS measurements were performed using the same process as that of FA. RLS spectra were acquired using an F-7100 spectrofluorometer (HITACHI, Japan).

2.5. Detection of FA vapor

The process for analyzing FA gas is illustrated in Fig. S1 (in Supporting Information). A bottle containing 250 μL CDs solution in a vial at the bottom was sealed. FA solutions with

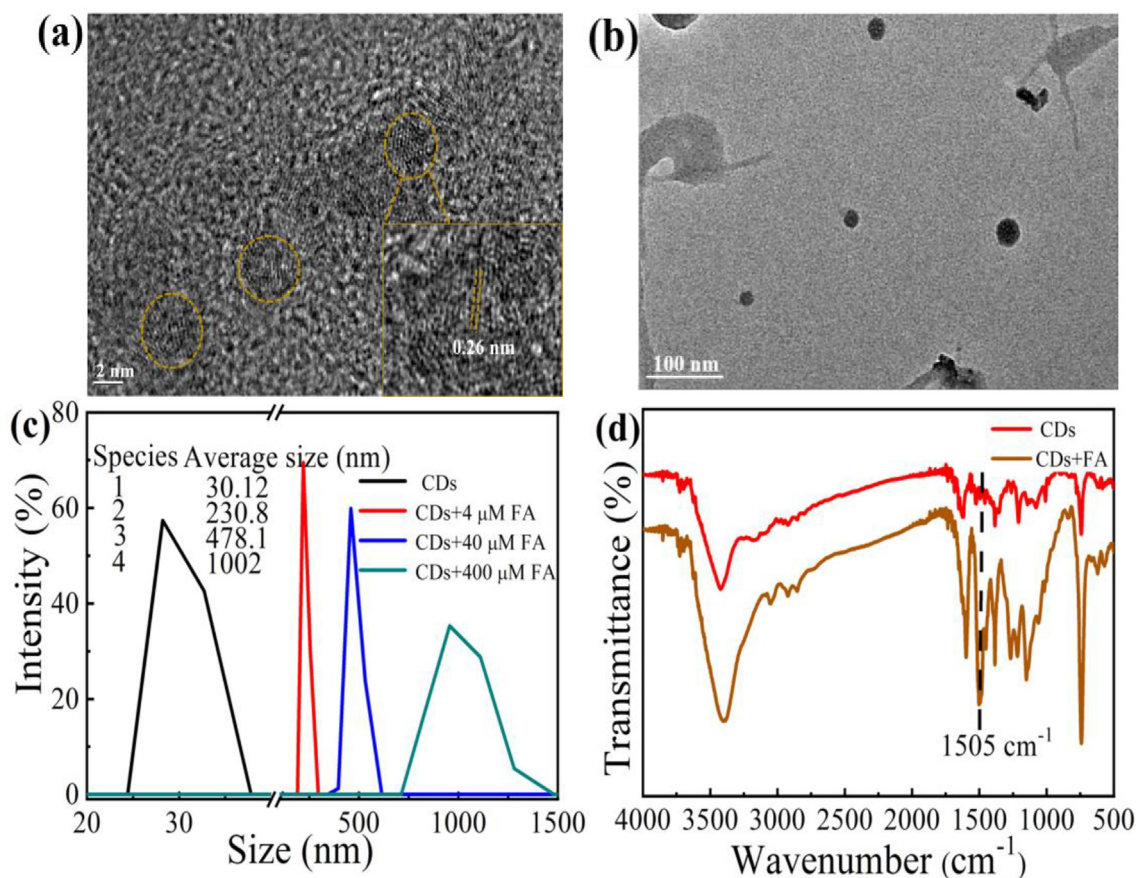


Fig. 1 TEM images of CDs (a), CDs + FA (b), dynamic light scattering (DLS) (c) and FT-IR spectrum (d) of CDs and CDs + FA.

different concentrations were dropped to the bottle bottom. The bottle was placed into a 50 °C water-bath to accelerate gasification of the FA solution (about 8 min) and the CDs solution was allowed to react completely with FA gas at room temperature for 18 min. Subsequently, the RLS spectra of the mixture solution were recorded.

2.6. Detection of FA in food samples

The standard addition method was used to determine FA, and the recovery was calculated. A small shrimp sample as food samples was triturated and weighed. The shrimp sample (1.5 g) and deionized water (100 mL) were combined in a 250 mL iodine volumetric flask. The mixture sample was treated with ultrasound and centrifugation (10000 rpm) for 20 min and 10 min, respectively. The supernatant of the sample was collected. CDs (1.25 mL), supernatant (0.15 mL), and the standard solutions of FA with different volumes were added to 7.34 mL of deionized water, and diluted to 250 μ L. After incubation for 20 min, the RLS spectra were recorded for the mixture solution of CDs and shrimp sample with and without the FA standard solution, respectively.

3. Results and discussion

3.1. Characterization

Fig. 1a, b and Fig. S2 a, b (in Supporting Information) show the TEM images of the CDs before and after the reaction with FA, respectively. CDs were freely dispersed in the aqueous medium without aggregation (Fig. 1a, Fig. S2 a, b). The morphology of the CDs is almost spherical, with a average particle size of 3.5 ± 0.4 nm ranging from 2.9 to 4.1 nm. The HR-TEM image exhibited CDs with a lattice parameter of 0.26 nm. When FA (0.4 μ M) was added to the CDs solution, the particle size of the CDs clearly increased, with medial diameter of 25 nm (Fig. 1b). DLS data for the CDs in the presence and absence of FA also confirm aggregation of the CDs with FA (Fig. 1c). Fig. 2c, the hydration diameter of the CDs was determined as ~ 30 nm, while the hydrodynamic size of the CDs was about 230, 478, and 1002 nm in the presence of 4, 40, and 400 μ M FA, respectively. It is deduced that FA can induce aggregation of the CDs, where aggregation becomes more extensive with increasing FA concentration. The FT-IR

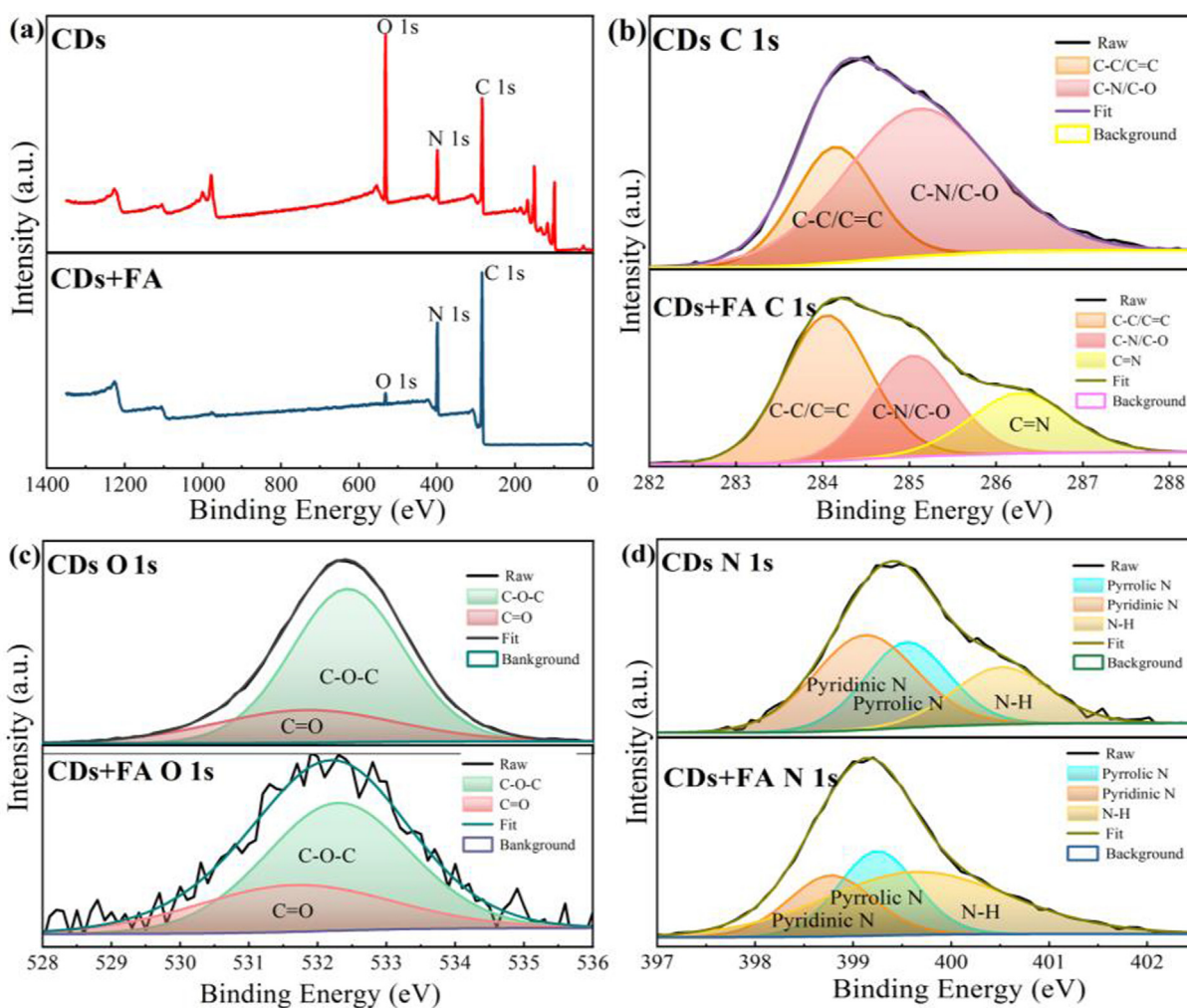


Fig. 2 XPS survey profile (a), C 1 s spectrum (b), O 1 s spectrum (c), and N 1 s spectrum (d) of the CDs (upper panels) and CDs + FA (lower panels).

spectra of the CDs and CDs + FA have two absorption bands at 3423 cm^{-1} and 1598 cm^{-1} (Fig. 1d), associated with N–H and C = O stretching vibrations, respectively (Zhao et al., 2019). The spectrum of CDs only shows a tiny band at 1505 cm^{-1} , whereas that of the CDs + FA has a distinct sharp peak owing to C = N stretching vibrations (Wu et al., 2018). It is obvious that FA can be easily captured by CDs owing to the covalent crosslink. XRD patterns of CDs (Fig. S3, in Supporting Information) shows a broad diffraction peak (002) at $2\theta = 24.5^\circ$, which is consistent with the graphitic structure (Hu et al., 2020). XPS was used to study the chemical bonds and chemical compounds on the surface of the CDs and CDs + FA. The XPS profile of the CDs (upper part, Fig. 2a) shows three typical peaks at 284.75, 399.18, and 532.11 eV, corresponding to C 1s, N 1s, and O 1s, respectively (An et al., 2021; Hu et al., 2020; Dai and Hu, 2022). The XPS profile of the CDs + FA (lower part) shows three main peaks at 284.91, 399.25, and 532.16 eV, which are assigned to C 1s, N 1s, and O 1s, respectively (An et al., 2021; Hu et al., 2020). The XPS data indicate that the CDs and CDs + FA comprise the same elements. The C 1s spectrum of the CDs (Fig. 2b) shows two peaks at 284 and 285 eV, corresponding to C–C/C = C and C–N/C–O, respectively (Yuan et al., 2021; Hu et al., 2020; Wang et al., 2019a). The O 1s spectrum of the CDs (Fig. 2c, upper part) shows two peaks at 531.8 and 532.3 eV, derived from C = O and C–O–C (Dong et al., 2022; Zhao et al., 2019), respectively. The N 1s spectrum of the CDs (Fig. 2d upper part) shows three peaks at 398.7, 399.2, and 400.4 eV, which results from pyrrolic N, pyridinic N, and N–H, respectively

(Dong et al., 2022; Li et al., 2022). The C 1s spectrum of the CDs + FA (Fig. 2b, lower part) shows three peaks at 284.1, 285, and 286.5 eV, owing to C–C/C = C, C–N/C–O, and C = N, respectively (Hu et al., 2020; Wu et al., 2018; Wang et al., 2019a, 2019b). The O 1s XPS spectrum of the CDs + FA (Fig. 2c, lower part) shows two peaks at 531.8 and 532.3 eV, attributed to C = O and C–O–C (Dong et al., 2022; Zhao et al., 2019), respectively. The N 1s spectrum of the CDs + FA (Fig. 2d, lower part) shows three peaks at 398.8, 399.2, and 399.7 eV, which are attributed to pyrrolic N, pyridinic N, and N–H, respectively (Dong et al., 2022; Li et al., 2022; Hu et al., 2021). Comparison of the XPS profiles of the CDs and CDs + FA shows a significant difference in the C 1s spectra (Fig. 2b). In the C 1s XPS spectrum of the CDs + FA, a new peak appeared at 286.5 eV. This new peak is ascribed to the formation of the C = N group via the Schiff-base reaction between CDs and FA. Therefore, FA can be easily captured by the CDs via covalent crosslinking of the aldehyde and amino groups of FA and the CDs to form covalent bonds.

3.2. Optical properties of CDs

Fig. 3 shows the optical properties of the CDs. The absorption bands at 232 nm and 285 nm in the spectra of the CDs and CDs + FA (Fig. 3a) are attributed to the π – π^* transition of the C = C bond, and the absorption peak at 420 nm is attributed to the n – π^* transition of C = N. The absorption band at 420 nm was absent in the spectrum of FA. When FA was

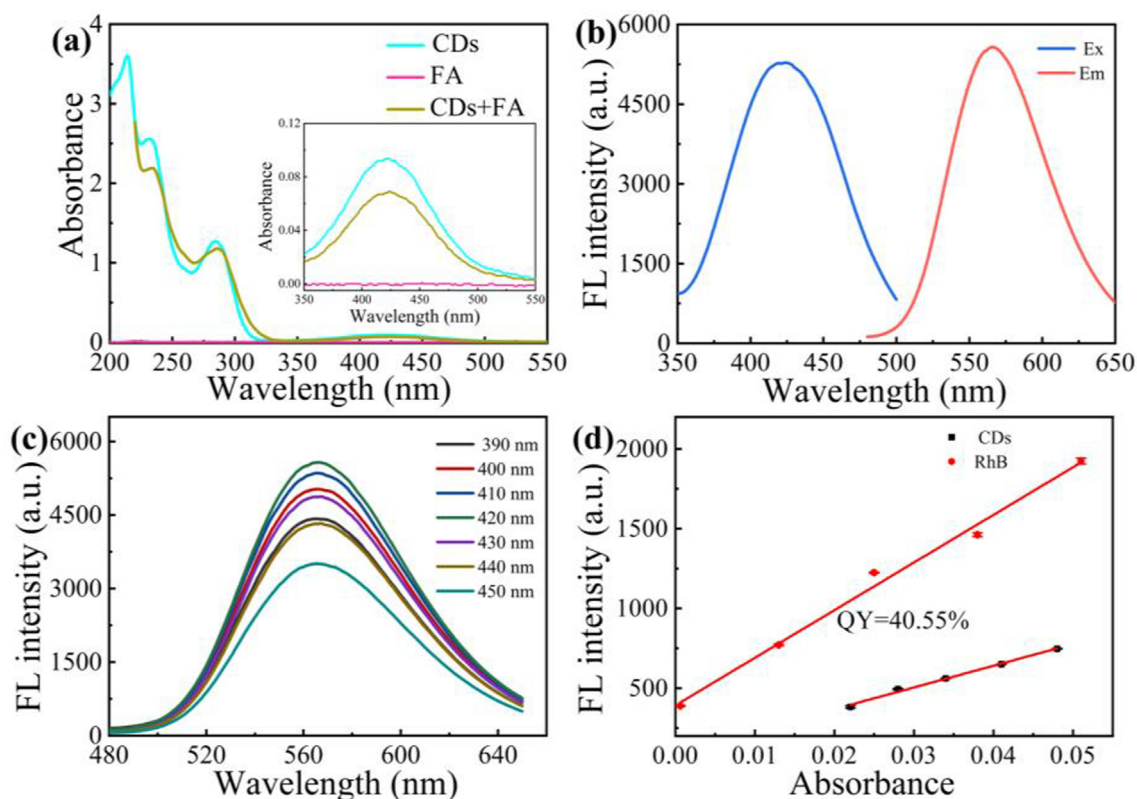


Fig. 3 Absorption spectra of CDs, FA, and CDs + FA (a); excitation and emission spectra of CDs (b); effect of excitation wavelength on the emission spectra of CDs (c); QY for CDs with Rh B as reference (d).

added to the CDs solution, the absorption peak of the CDs clearly decreased (inset of Fig. 3a) due to the formation of precipitates of CDs in the reaction of CDs and FA. Fig. 3b shows the excitation/emission peaks of the CDs at 419/567 nm. When the excitation wavelength was changed from 390 nm to 450 nm (Fig. 3c), the emission peak at 567 nm showed excitation-independent fluorescence characteristics. With Rhodamine B (RhB) as the reference, the quantum yield (QY) of the CDs was measured (Fig. 3d). The QY of the CDs was ~ 0.41 .

3.3. Detection of FA

3.3.1. Detection of FA in aqueous media

First, the stability of CDs was studied. As shown in Fig. S4a (in Supporting Information), the CDs of RLS intensity changes in the pH range of 2–12, but it can be seen that the CDs of RLS intensity remains basically stable in the range of 5–9. Different concentrations of NaCl solutions were used to study the effect of ionic strength (Fig. S4b, in Supporting Information). CDs have no distinct RLS changes in NaCl solutions (0–100 mM). In addition, the RLS of CDs is basically stable for seven days (Fig. S4c, in Supporting Information).

Second, the precursor of CDs and other CDs were tested for the detection of FA. When FA solutions with different concentrations (4 nM–1.6 mM) were added to OPA solution, the RLS signal has a neglectable increase (Fig. S5a, in Supporting

Information). Nitrogen-doped CDs (N-CDs) are usually amino-rich CDs, are these CDs all suitable to detect FA by RLS through Schiff-base reaction? The N-CDs were obtained using the previous method (Arkin et al., 2021). When FA solutions (4 nM–400 μ M) were added to the N-CDs solution, the RLS signal of the N-CDs has not distinct change (Fig. S5b and c, in Supporting Information). Thus, our CDs rather than the precursor and the N-CDs can be used for detecting FA.

Third, the selectivity of the present CDs system for FA detection was investigated. Common organic molecules with similar structure as FA were studied. They included AA, PA, BA, GA, HP, MeOH, EtOH, Ace and Glu. The RLS intensity for the CDs with all these species is shown in Fig. 4a and b. Clearly, these molecules have no obvious influence on the RLS intensity of CDs.

Fourth, the reaction time between CDs and FA was optimized (Fig. S5d in Supporting Information). The RLS intensity was recorded after mixing CDs and FA for different time. The RLS intensity of CDs + FA increases with reaction time, and gets to a platform after 18 min. Thus, the interaction of CDs and FA can finish within 18 min.

Finally, the sensitivity of the CDs system for FA detection was studied. When FA solution (4 nM–1.6 mM) was added to CDs solution, the RLS signal of the CDs was distinctly enhanced (Fig. 4c). As shown in Fig. 4d, the RLS intensity of the CDs at ~ 346 nm increased with the FA concentration in the range of 4 nM–1.6 mM. The increment of RLS intensity

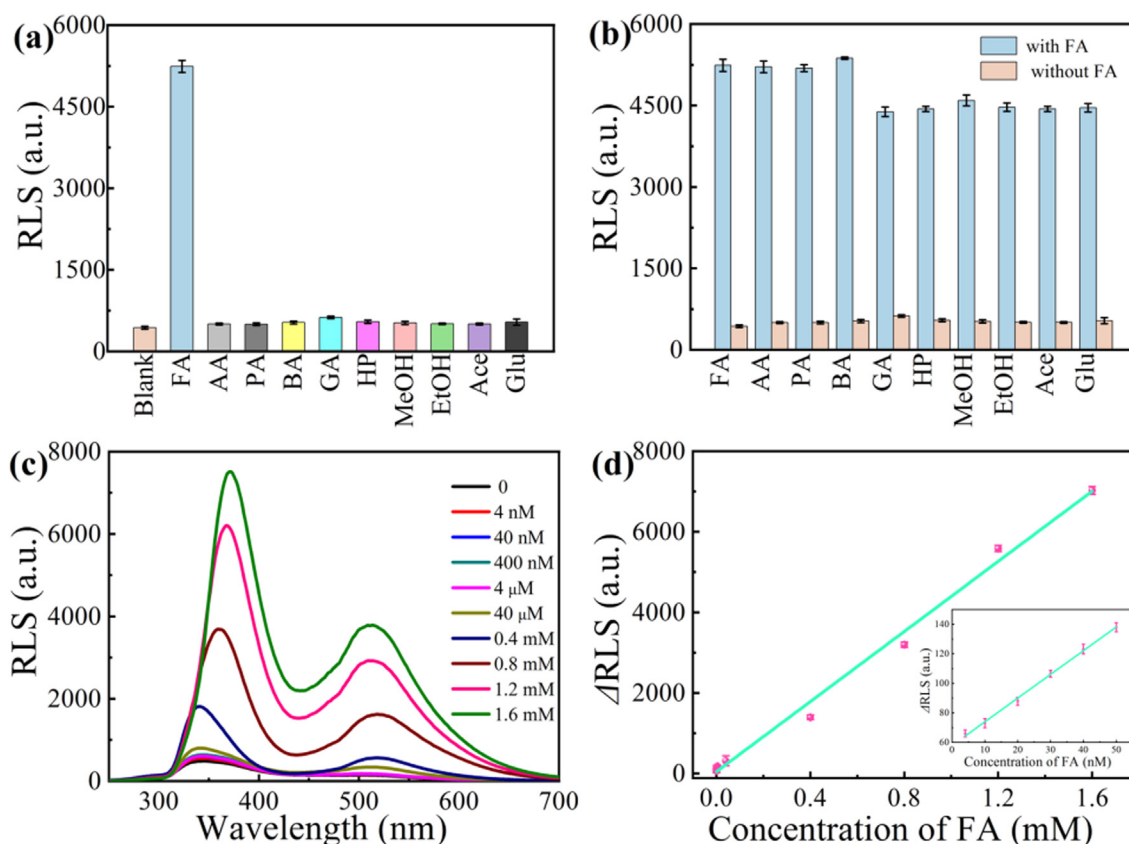


Fig. 4 RLS intensity at ~ 346 nm with and without different molecules (a), and effect of various other molecules on the response of CDs to FA (b), RLS spectra of CDs in the presence of FA with different concentrations (c), and corresponding linear relationship between Δ RLS and concentration of FA (the inset shows the relationship at low FA concentration) (d) (the concentration of FA, AA, PA, BA, GA, HP, MeOH, EtOH, Ace, MeOH, EtOH, Ace, and Glu is 1.2 mM).

(Δ RLS) exhibits a linear relationship to the FA concentration with the linear regression equation: Δ RLS = 4351.24 [FA] + 46.28 ($R^2 = 0.992$). Δ RLS and [FA] represent the RLS increment of CDs with FA, and the FA concentration, respectively. In the range of 4–50 nM, the RLS signal of CDs also was enhanced (Fig. S6, in Supporting Information) and the linearity is better ($R^2 = 0.996$) (inset of Fig. 4D). The limit of detection (LOD) is 1.6 nM, which is estimated using equation of $3S_B/m$ (Hou et al., 2020).

The results from the proposed and the previous methods for FA detection are listed in Table S1 (in Supporting Information). The present method has a wider linear range and a lower LOD than most of the other methods.

3.3.2. Detection of FA vapor

FA vapor was detected using a lab-made device (Fig. S1, in Supporting Information). The small molecules were volatilized into gases at a concentration of 10 μ M (within 8 min) (Gu et al., 2020). The concentration of FA vapor can be determined by applying the Eq. (1).

$$C = (22.4\rho TV_s \times 10^3)/273MV$$

In Eq. (1), C is the concentration of FA (ppm), ρ is the density of liquid FA (g mL^{-1}), T is the temperature where the test is performed (K), V_s is the volume of liquid FA (μ L), M is the molecular weight (g mol^{-1}), and V is the volume of the device (L).

The specificity for FA is tested using the molecules with similar structure of AA, PA, BA, GA, HP, MeOH, EtOH, Ace and Glu as interferences (Fig. 5a and b). It is obvious that the CDs have high selectivity for the detection of FA vapor.

FA in vapor samples with different concentrations (0.04–10 μ M) was detected (Fig. 5c). The RLS intensity at \sim 346 nm of CDs increases with the concentration of FA vapor and the corresponding relationship is linear in the range of 0.04–10 μ M (Δ RLS = 69.58 [FA] (μ M) + 58.48, $R^2 = 0.996$) (Fig. 5d). The LOD was 32.33 nM using the equation $3S_B/m$. The present method is compared with previous reports for the detection of FA vapor (Table S2), indicating that the present RLS method owns a wider linear range and lower LOD.

3.4. Applications

FA is widely used as a preservative in food. If people eats food contaminated FA for a long time, even though can cause numerous diseases (Zhang et al., 2022a, 2022b). Therefore, it is necessary to determine FA in food samples.

The developed method is expected to be useful for practical analysis in real samples. Herein, shrimp samples were used as real samples. After appropriate preprocessing, FA in small shrimp samples was determined (Table 1). The recovery is ranging from 99.5 to 105.8%, with a relative standard deviation (RSD) of less than 6.7%. The concentration of FA in real

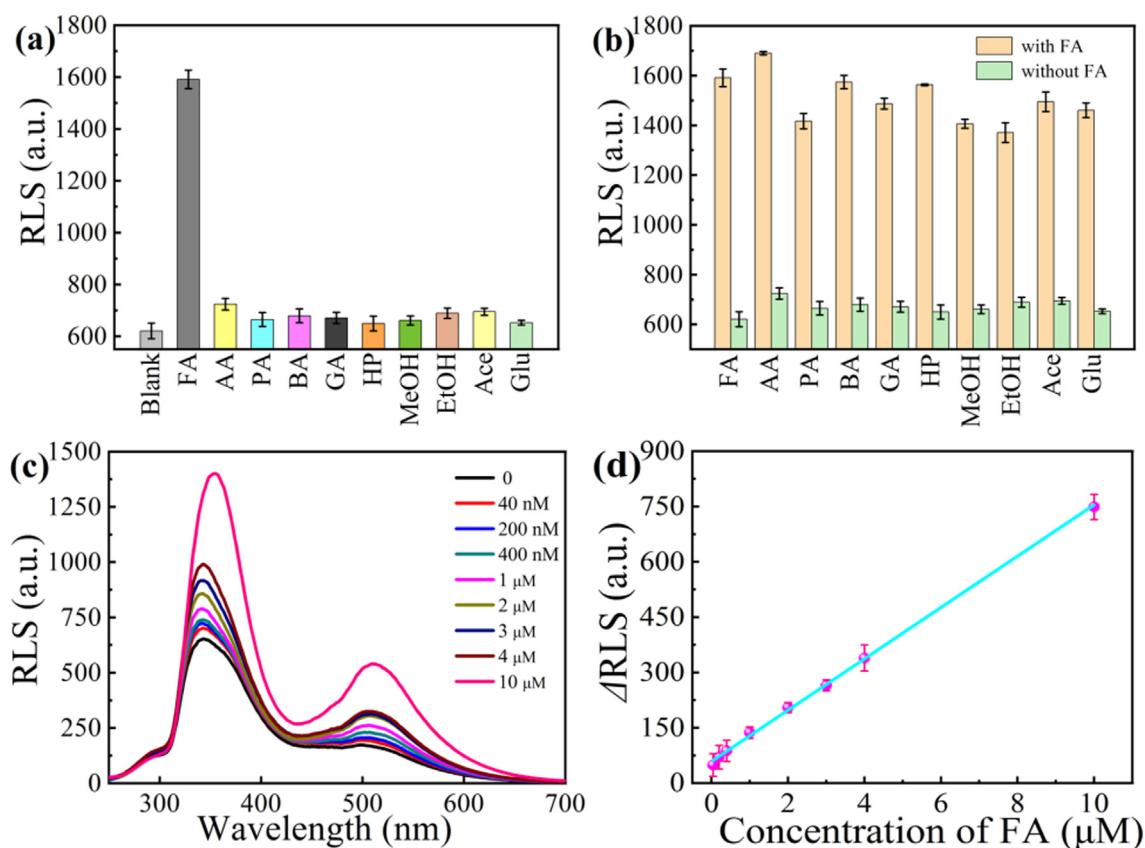


Fig. 5 RLS intensity at \sim 346 nm with and without various gas molecules (a), and effect of various other molecules on the response of CDs to FA gas at room temperature (b). RLS spectra of CDs in the presence of FA gas with different concentrations (c), and corresponding linear relationship between Δ RLS and the concentration of FA gas (d) (the concentration of FA, AA, PA, BA, GA, HP, MeOH, EtOH, Ace and Glu is 10 μ M).

Table 1 Determination of FA in real samples.

Sample	Spiked ($\mu\text{g}\cdot\text{g}^{-1}$)	Found ($\mu\text{g}\cdot\text{g}^{-1}$)	Spectrophotometry ($\mu\text{g}\cdot\text{g}^{-1}$)	Recovery (%) (n = 3)	RSD (%)
Shrimp	0	2.45	2.72	—	5.5
	5.3	8	8.27	104.1%	6.7
	21.3	23.67	24.27	99.5%	2.5
	26.7	30.67	29.6	105.8%	4.3

sample of shrimp is $1.2 \mu\text{M}$. By calculation, the content of FA is $2.72 \mu\text{g}\cdot\text{g}^{-1}$ in shrimp.

3.5. Possible mechanism

As shown in Fig. 2d and 3b, there are numerous amino groups on the surface of CDs. Owing to covalent crosslinking via the Schiff-base reaction (Ge et al., 2020), FA reacts with the amino groups on the surface of the CDs to form C = N bonds (Fig. 2e and 3b). Formation of the C = N bond reduces the solubility of CDs products in aqueous medium. Therefore, the nanoparticles of CDs can aggregate in the presence of FA, and even instantly form precipitates (Chen et al., 2019c). These precipitates bring about the enhancement of the RLS signal. The enhancement of RLS signal is linearly responsive to the concentration of FA. Thus, a sensitive and selective RLS method was developed for sensing FA.

4. Conclusions

In summary, a RLS method was developed for the simultaneous detection of FA in aqueous and vapor medium. The RLS technique not only has high sensitivity, but also offers high selectivity, aiding the study of molecules and nanomaterials assembly. CDs were used as RLS probes for FA capture. CDs exhibit yellow fluorescence, with a medium QY of ~ 0.41 . The optical features, morphology, and surface groups of the CDs were examined. The surface of CDs is rich in amino groups, derived mainly from OPD. In the presence of FA, CDs undergo obvious aggregation due to the covalent crosslinking of FA via the Schiff-base reaction, thereby inducing RLS signal enhancement. The increase in the RLS intensity exhibits a sensitive, selective, and linear response to FA. The proposed CDs system was used to assay FA in shrimp samples. This study highlights the possibility of extending CDs to the capture of FA in food field.

Declaration of Competing Interest

The authors declare that they have no known competing financial interests or personal relationships that could have appeared to influence the work reported in this paper.

Acknowledgments

This work was supported financially by Natural Science Foundation of Shandong Province (ZR2022MB052), Graduate Education Quality Improvement Plan of Shandong Province (SDYJG21198), and the College Students' Innovation and Entrepreneurship Training Program (CXC2022206) and research foundation of Liaocheng University (318050022 and 318012116).

Appendix A. Supplementary data

Supplementary data to this article can be found online at <https://doi.org/10.1016/j.arabjc.2023.104786>.

References

- An, Y., Lin, X., Zhou, Y., Li, Y., Zheng, Y., Wu, C., Xu, K., Chai, X., Liu, C., 2021. Red, green, and blue light-emitting carbon dots prepared from o-phenylenediamine. *RSC Adv.* 43, 26915–26919.
- Aquilina, G., Bampidis, V., 2014. Scientific Opinion on the safety and efficacy of formaldehyde for all animal species based on a dossier submitted by Regal BV. *EFSA J.* 12, 3561–3587.
- Arkin, K., Zheng, Y., Hao, J., Zhang, S., Shang, Q., 2021. Polychromatic Carbon Dots Prepared from m-Phenylenediamine and Urea as Multifunctional Fluorescent Probes. *ACS Appl. Nano Mater.* 4, 8500–8510.
- Bi, A., Gao, T., Cao, X., Dong, J., Liu, M., Ding, N., Liao, W., Zeng, W., 2018. A novel naphthalimide-based probe for ultrafast, highly selective and sensitive detection of formaldehyde. *Sens. Actuators B Chem* 255, 3292–3297.
- Chang, X., Wu, X., Guo, Y., Zhao, Y., Zheng, J., Li, X., 2018. SnSO₄ modified ZnO nanostructure for highly sensitive and selective formaldehyde detection. *Sens. Actuators B Chem* 255, 1153–1159.
- Chen, H., Huang, C., Ding, Y., Zhang, Q.L., Zhu, B.X., Ni, X.L., 2019c. Organic core-shell-shaped micro/nanoparticles from twisted macrocycles in Schiff base reaction. *Chem. Sci.* 10, 490–496.
- Chen, W., Ji, D., Zhang, Y., Xu, P., Gao, X., Fang, J., Li, X., Feng, L., Wen, W., 2019a. Schiff-base reaction induced selective sensing of trace dopamine based on a Pt₄₁Rh₅₉ alloy/ZIF-90 nanocomposite. *Nanotechnology* 30, 335708–335715.
- Chen, S., Jia, Y., Zou, G.Y., Yu, Y.L., Wang, J.H., 2019b. A ratiometric fluorescent nanoprobe based on naphthalimide derivative-functionalized carbon dots for imaging lysosomal formaldehyde in HeLa cells. *Nanoscale* 11, 6377–6383.
- Chen, F., Liu, Y., Liao, R., Gong, H., 2017. Reduced graphene oxide as a resonance light-scattering probe for thrombin detection using dual-aptamer-based dsDNA. *Anal. Chim. Acta* 985, 141–147.
- Chen, F., Zhang, F., Liu, Y., Cai, C., 2018. Simply and sensitively simultaneous detection hepatocellular carcinoma markers AFP and miRNA-122 by a label-free resonance light scattering sensor. *Talanta* 15, 473–480.
- Dai, R., Hu, Y., 2022. Green/red dual emissive carbon dots for ratiometric fluorescence detection of acid red 18 in food. *Sens. Actuators B Chem* 370, 132420–132426.
- Dong, Y., Li, T., Bateer, B., Wang, H., Fu, Q., Zhang, F., 2022. Preparation of yellow emissive nitrogen-doped carbon dots from o-phenylenediamine and their application in curcumin sensing. *New J. Chem.* 20, 9543–9549.
- Du, L., Li, Y., Tong, Y., Zhang, M., 2021. Biotemplates based preparation of hierarchical ZnSnO₃ porous nanostructures for fast detection of formaldehyde. *Ceram. Int.* 47, 13139–13146.
- Gakhar, T., Hazra, A., 2021. C₆₀-encapsulated TiO₂ nanoparticles for selective and ultrahigh sensitive detection of formaldehyde. *Nanotechnology* 32, 505505.
- Gao, S., Wang, X., Xu, N., Lian, H., Xu, L., Zhang, W., Xu, C., 2021. From coconut petiole residues to fluorescent carbon dots via a

- green hydrothermal method for Fe³⁺ detection. *Cellul.* 28, 1647–1661.
- Ge, H., Liu, G., Yin, R., Sun, Z., Chen, H., Yu, L., Su, P., Sun, M., Alamry, K.A., Marwani, H.M., Wang, S., 2020. An aldimine condensation reaction based fluorescence enhancement probe for detection of gaseous formaldehyde. *Microchim. J.* 156, 104793–104799.
- Gorrotxategi-Carbajo, P., Fasci, E., Ventrillard, I., Carras, M., Maisons, G., Romanini, D., 2013. Optical-feedback cavity-enhanced absorption spectroscopy with a quantum-cascade laser yields the lowest formaldehyde detection limit. *Appl. Phys. B* 110, 309–314.
- Gu, D., Yang, W., Lin, D., Qin, X., Yang, Y., Wang, F., Pan, Q., Su, Z., 2020. Water-stable lanthanide-based metal-organic gel for the detection of organic amines and white-light emission. *J. Mater. Chem. C* 8, 13648–13654.
- Hou, Y., Liu, J., Hong, M., Li, X., Ma, Y., Yue, Q., Li, C.-Z., 2017. A reusable aptasensor of thrombin based on DNA machine employing resonance light scattering technique. *Biosens. Bioelectron.* 92, 259–265.
- Hou, Y., Liu, H., Li, Z., Zhang, H., Wei, L., Yu, M., 2020. One-step synthesis of mitochondrion-targeted fluorescent carbon dots and fluorescence detection of silver ions. *Anal. Methods* 12, 2835–2840.
- Hu, Y., Gao, Z., 2020. Sewage sludge in microwave oven: A sustainable synthetic approach toward carbon dots for fluorescent sensing of para-Nitrophenol. *J. Haz. Mat.* 382, 121048–121055.
- Hu, Y., Guan, R., Zhang, C., Zhang, K., Liu, W., Shao, X., Xue, Q., Yue, Q., 2020. Fluorescence and photocatalytic activity of metal-free nitrogen-doped carbon quantum dots with varying nitrogen contents. *Appl. Surf. Sci.* 531, 147344.
- Hu, Y., Gao, Z., Luo, J., 2021. Fluorescence detection of malachite green in fish tissue using red emissive Se, N, Cl-doped carbon dots. *Food Chem.* 335, 127677–127683.
- Kim, N., Lee, J., Gu, M., Kim, B.S., 2021. Modulating charge carriers in carbon dots toward efficient solar-to-energy conversion. *Carbon Energy* 3, 590–614.
- Li, Y., Hu, M., Liu, K., Gao, S., Lian, H., Xu, C., 2023. Lignin derived multicolor carbon dots for visual detection of formaldehyde. *Ind. Crop. Prod.* 192, 116006–116017.
- Li, P., Xue, S., Sun, L., Zong, X., An, L., Qu, D., Wang, X., Sun, Z., 2022. Formation and fluorescent mechanism of red emissive carbon dots from o-phenylenediamine and catechol system. *Light: Sci. Appl.* 11, 298.
- Lin, Y., Lin, P., Hsieh, S., Tsai, C., 2022. Quantum Dot Assisted Precise and Sensitive Fluorescence-Based Formaldehyde Detection in Food Samples. *Spectrochim. Acta A: Mol. Biomol. Spectrosc.* 283, 121729–121737.
- Liu, H., Sun, Y., Li, Z., Yang, J., Aryee, A.A., Qu, L., Du, D., Lin, Y., 2019. Lysosome-targeted carbon dots for ratiometric imaging of formaldehyde in living cells. *Nanoscale* 11, 8458–8463.
- Liu, Y., Wang, H., Li, S., Gong, H., 2018. Ultrasensitive detection of thrombin based on MoS₂-aptamer biosensors by resonance light scattering technique. *Sens. Actuators B Chem.* 258, 402–407.
- Liu, Y., Roy, S., Sarkar, S., Xu, J., Zhao, Y., Zhang, J., 2021. A review of carbon dots and their composite materials for electrochemical energy technologies. *Carbon Energy* 3, 795–826.
- Lu, W., Fernández Band, B.S., Yu, Y., Geng Li, Q., Chuan Shang, J., Wang, C., Fang, Y., Tian, R., Ping Zhou, L., Li Sun, L., Tang, Y., Hua Jing, S., Huang, W., Ping Zhang, J., 2006. Resonance light scattering and derived techniques in analytical chemistry: past, present, and future. *Microchim. Acta* 158, 29–58.
- Luo, D., Chen, B., Li, X., Liu, Z., Liu, X., Liu, X., Shi, C., Zhao, X.S., 2018. Three-dimensional nitrogen-doped porous carbon anchored CeO₂ quantum dots as an efficient catalyst for formaldehyde oxidation. *J. Mater. Chem. A* 6, 7897–7902.
- Luo, L., Yang, J., Liang, K., Chen, C., 2019. Fast and sensitive detection of Japanese encephalitis virus based on a magnetic molecular imprinted polymer-resonance light scattering sensor. *Talanta* 202, 21–27.
- Luo, L., Zhang, F., Cai, C., 2020. Molecular imprinting resonance light scattering nanoprobe based on pH-responsive metal-organic framework for determination of hepatitis A virus. *Microchim. Acta* 140, 140–148.
- Nordin, N., Fatimah, A., Farhana, Y., 2011. Formaldehyde content and quality characteristics of selected fish and seafood from wet markets. *Food Res. J.* 18, 125–136.
- Padmalaya, G., Vardhan, K.H., Kumar, P.S., Ali, M.A., Chen, T.W., 2022. A disposable modified screen-printed electrode using egg white/ZnO rice structured composite as practical tool electrochemical sensor for formaldehyde detection and its comparative electrochemical study with Chitosan/ZnO nanocomposite. *Chemosphere* 288, 132560–132569.
- Papaioannou, N., Titirici, M., Sapelkin, A., 2019. Investigating the Effect of Reaction Time on Carbon Dot Formation, Structure, and Optical Properties. *ACS Omega* 26, 21658–21665.
- Park, S.J., Bae, I., Nam, I.-S., Cho, B.K., Jung, S.M., Lee, J.-H., 2012. Oxidation of formaldehyde over Pd/Beta catalyst. *Chem. Eng. J.* 195, 392–402.
- Qu, J., Zhang, X., Liu, Y., Xie, Y., Cai, J., Zha, G., Jing, S., 2020. N, P-co-doped carbon dots as a dual-mode colorimetric/ratiometric fluorescent sensor for formaldehyde and cell imaging via an amination reaction-induced aggregation process. *Microchim. Acta* 187, 355–365.
- Song, Y., Gao, C.Y., Qiao, L., Fan, S.H., 2009. A Sequential Injection Method Coupled with Chemiluminescence Detection for the Determination of Formaldehyde in Air. *Chinese phys. C* 30, 467–472.
- Vedernikova, A., Miruschenko, M., Arefina, I., 2022. Dual-Purpose Sensing Nanoprobe Based on Carbon Dots from o-Phenylenediamine: pH and Solvent Polarity Measurement. *Nanomaterials* 12, 3314–3328.
- Visuvamithiran, P., Palanichamy, M., Shanthi, K., Murugesan, V., 2013. Selective epoxidation of olefins over Co(II)-Schiff base immobilised on KIT-6. *Appl. Catal. A* 462, 31–38.
- Wang, T., Chen, G., Li, L., Wu, Y., 2019a. Highly Fluorescent Green Carbon Dots as a Fluorescent Probe for Detecting Mineral Water pH. *Sensors* 19, 3801–3811.
- Wang, Y., Liu, Y., Zhou, J., Yue, J., Xu, M., An, B., Ma, C., Li, W., Sun, S., 2021. Hydrothermal synthesis of nitrogen-doped carbon quantum dots from lignin for formaldehyde determination. *RSC Adv.* 11, 29178–29185.
- Wang, J., Xue, J., Xiao, X., Xu, L., Jiang, M., Peng, P., Liao, L., 2017. Determination of thorium (IV) using isophthalaldehyde-tetrapyrrole as probe by resonance light scattering, second-order scattering and frequency-doubling scattering spectra. *Spectrochim. Acta A* 187, 104–109.
- Wang, S., Zhang, F., Chen, C., Cai, C., et al., 2019b. Ultrasensitive graphene quantum dots-based catalytic hairpin assembly amplification resonance light scattering assay for p53 mutant DNA detection. *Sens. Actuators B Chem* 15, 42–47.
- Wen, L., Ao, S., Yueqi, L., Hao, Z., Xiaohui, H., Xueliang, L., Xinchao, S., Yunxu, Y., 2020. The selective and sensitive detection of formaldehyde by ZIF-90-LW via aza-Cope rearrangement. *Anal. Methods* 12, 3748–3755.
- Wu, B., Shi, X., Han, W., Wang, T., Wang, C., 2018. A double fluorescent nanoprobe based on phosphorus/nitrogen co-doped carbon dots for detecting dichromate ions and dopamine. *RSC Adv.* 8, 31793–31802.
- Yang, B., Gong, H., Chen, C., Chen, X., Cai, C., 2017. A virus resonance light scattering sensor based on mussel-inspired molecularly imprinted polymers for high sensitive and high selective detection of Hepatitis A Virus. *Biosens. Bioelectron.* 87, 679–685.
- Yuan, C., Qin, X., Xu, Y., Shi, R., Cheng, S., Wang, Y., 2021. Dual-signal uric acid sensing based on carbon quantum dots and o-

- phenylenediamine. *Spectrochim. Acta A Mol. Biomol. Spectrosc.* 254, 119678.
- Zaltariov, M.-F., Cazacu, M., 2020. Coordination compounds with siloxane/silane-containing ligands capable of self-assembly at nano/micro scale in solid state and in solution. *Nan. Coord. Chem* 8, 155–196.
- Zhang, S., Wen, X., Long, M., Xi, J., Hu, J., Tang, A., 2020b. Fabrication of CuO/Cu/TiO₂ nanotube arrays modified electrode for detection of formaldehyde. *J. Alloy. Compd.* 829, 154568–154577.
- Zhang, H., Wu, Z., Zhi, Z., Gao, W., Sun, W., Hua, Z., Wu, Y., 2022a. Practical and Efficient: A Pocket-Sized Device Enabling Detection of Formaldehyde Adulteration in Vegetables. *ACS Omega* 7, 160–167.
- Zhang, S., Zhao, L., Huang, B., Li, X., 2020a. UV-activated formaldehyde sensing properties of hollow TiO₂@SnO₂ hetero-junctions at room temperature. *Sens. Actuators B Chem* 319, 128264.
- Zhang, H., Zheng, Z., Yu, T., Liu, C., Qian, H., Li, J., 2022b. Seasonal and diurnal patterns of outdoor formaldehyde and impacts on indoor environments and health. *Environ. Res.* 205, 112550–112558.
- Zhao, J., Li, F., Zhang, S., An, Y., Sun, S., 2019. Preparation of N-doped yellow carbon dots and N,P co-doped red carbon dots for bioimaging and photodynamic therapy of tumors. *New J. Chem.* 43, 6332–6342.
- Zhao, B., Ma, H., Zheng, M., Xu, K., Zou, C., Qu, S., Tan, Z.a., 2022. Narrow-bandwidth emissive carbon dots: A rising star in the fluorescent material family. *Carbon Energy* 4, 88–114.
- Zhou, L., Qian, R., Zhuo, S., Chen, Q., Wen, Z., Li, G., 2020. Oximation reaction induced reduced graphene oxide gas sensor for formaldehyde detection. *J. Saudi Chem. Soc.* 24, 364–373.